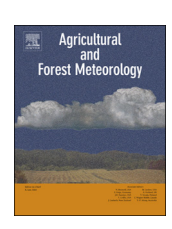
ELSEVIER

Contents lists available at ScienceDirect

Agricultural and Forest Meteorology

journal homepage: www.elsevier.com/locate/agrformet



Spatiotemporal sensitivity of thermal stress for monitoring canopy hydrological stress in near real-time



Bijan Seyednasrollah^{a,b,c,*}, Jean-Christophe Domec^{d,e}, James S. Clark^{d,f}

- ^a Department of Organismic and Evolutionary Biology, Harvard University, Cambridge, MA, 02138, USA
- b School of Informatics, Computing, and Cyber Systems, Northern Arizona University, Flagstaff, AZ, 86011, USA
- ^c Center for Ecosystem Science and Society, Northern Arizona University, Flagstaff, AZ, 86011, USA
- d Nicholas School of the Environment, Duke University, Durham, NC, 27708, USA
- e Bordeaux Sciences Agro, UMR 1391 INRA-ISPA, 33175, Gradignan Cedex, France
- f Department of Statistical Science, Duke University, Durham, NC, 27708, USA

ARTICLE INFO

Keywords: Thermal stress Remote sensing Evapotranspiration Bayesian Hierarchical modeling

ABSTRACT

Monitoring drought in real-time using minimal field data is a challenge for ecosystem management and conservation. Most methods require extensive data collection and in-situ calibration and accuracy is difficult to evaluate. Here, we demonstrated how the space-borne canopy "thermal stress", defined as surface-air temperature difference, provides a reliable surrogate for drought-induced water stress in vegetation. Using physics-based relationships that accommodate uncertainties, we showed how changes in canopy water flux from ground-based measurements relate to both the surface energy balance and remotely-sensed thermal stress. Field measurements of evapotranspiration in the southeastern and northwestern US verify this approach based on sensitivity of evapotranspiration to thermal stress in a large range of atmospheric and climate conditions. We found that a 1 °C change in the thermal stress is comparable to 1-1.2 mm day⁻¹ of evapotranspiration, depending on site and climate conditions. We quantified temporal and spatial sensitivity of evapotranspiration to the thermal stress and showed that it has the strongest relationship with evapotranspiration during warm and dry seasons, when monitoring drought is essential. Using only air and surface temperatures, we predicted the inter-annual anomaly in thermal stress across the contiguous United States over the course of 15 years and compared it with conventional drought indices. Among drought metrics that were considered in this study, the thermal stress had the highest correlation values. Our sensitivity results demonstrated that the thermal stress is a particularly strong indicator of water-use in warm seasons and regions. This simple metric can be used at varying time-scales to monitor surface evapotranspiration and drought in large spatial extents in near real-time.

1. Introduction

Increasing frequency, magnitude, and duration of droughts highlight the need for rapid assessment and monitoring (Clark et al., 2016; Tang et al., 2014; Vose et al., 2016). Increases in tree mortality (Allen et al., 2010), declines in forest health (Guarín and Taylor, 2005) and changes in species composition (Klos et al., 2009), are expected with increasing droughts (Novick et al., 2015; Schwantes et al., 2017). Deterministic energy balance methods for estimating land surface waterbudget have been continuously improved over the past decades (AghaKouchak et al., 2015; Bastiaanssen et al., 1998a, b; Mu et al., 2011; Wang and Dickinson, 2012). However, the spatiotemporal sensitivities of these approaches and their stochasticity are yet to be quantified (Bastiaanssen et al., 2005; Yang et al., 2013).

Challenges associated with direct measurement of evapotranspiration have motivated the development of techniques to simplify calculations and/or minimize the number of measurements needed to evaluate evapotranspiration. The current indices used to monitor evapotranspiration require extensive calibration (Courault et al., 2005) and are typically available only after the fact (Allen et al., 2011; Anderson et al., 2008; Beguería, 2017; Teixeira et al., 2009). Parametrization methods can be categorized into three approaches: climate-based, vegetation-based, and energy-based. Climate-based methods rely on atmospheric demand (e.g. vapor-pressure deficit) and do not consider the cumulative withdrawal of soil moisture by plants (Saha et al., 1986) (as imbedded in several drought severity indices such as *PDSI*, *SPI*, and *SPEI*). Vegetation-based methods estimate surface evapotranspiration from canopy spectral reflectance and vegetation indices,

^{*} Corresponding author at: School of Informatics, Computing, and Cyber Systems, Northern Arizona University, Flagstaff, AZ, 86011, USA. E-mail addresses: seyednasrollah@fas.harvard.edu, bijan.s.nasr@gmail.com (B. Seyednasrollah).

such as the normalized difference vegetation index (NDVI) (Nagler et al., 2003) (e.g., MODIS DSI). These methods suffer from errors that result from disturbance (Wardlow et al., 2016), such as forest harvest, pathogen and insect attack, or damage due to extreme climate events that are not associated with drought. Vegetation-based methods do not detect rapid changes in evapotranspiration, due to the delay between the onset of drought and plant response (Chiesi et al., 2013) (e.g., DSI and MODIS ET). Energy-based techniques conserve energy flux to and from the earth surface (Yang et al., 2013). In other words, surface energy indicators can be used as reliable surrogates to monitor the rate of evapotranspiration (Kustas et al., 2011) and identify drought induced water stressed areas (Anderson et al., 2008; Kustas and Anderson, 2009), at large spatial extents (Norman et al., 2016), Although, deterministic energy-based methods have been used in monitoring evapotranspiration at different scales (Anderson et al., 2007; Norman et al., 1995) and for different vegetation densities (French et al., 2005; Li et al., 2005), stochastic approaches can improve the accuracy of these models for varying conditions (Timmermans et al., 2007). However, our understanding of the accuracy of these methods under different conditions and ecoregions remains limited (Liou and Kar, 2014; Abbaszadeh et al., 2018).

Surface energy balance can be described by the equality

$$\lambda ET_{s,t} = R_{s,t} + LI_{s,t} - LO_{s,t} - H_{s,t}$$

where R, LI, and LO are net absorbed solar (shortwave) and incoming and outgoing thermal (longwave) radiation, respectively. H is the sensible heat flux, related to changes in the surface temperature, λ is the specific latent heat of vaporization, and ET is the rate of evapotranspiration for location s and at time t (here taken in days). Ground heat flux is accommodated as a loss in the R term (Choudhury et al., 1987).

ET can be obtained from the energy balance equation when all other energy components are known, but this is generally not the case (Price. 1980). R. LI. LO and H depend on other physical parameters of the surface and atmosphere. In this section, we explain each energy component and how they are related to the surface and atmospheric properties. R depends on the surface albedo, canopy transmissivity, and heat loss to the ground. R follows the relationship $R_{s,t} = \alpha_s SI_{s,t}$, where α_s is the canopy absorption factor at site s, and SI is the incoming solar radiation. LI and LO are related to sky and surface emissivity and surface (TS) and air (TA) temperatures by the Stefan-Boltzmann law (Seyednasrollah and Kumar, 2013). Emissivity is the dimensionless measure of ability to emit thermal energy. For simplicity, we assumed broadband emissivity across wavelengths. Sky emissivity (ɛsky) ranges from 0.6 for clear sky to above 0.9 for overcast (Flerchinger et al., 2009; Prata, 1996; Seyednasrollah et al., 2013). While land surface emissivity can vary largely depending on land use and conditions (Badenas, 1998; Caselles et al., 1997; Jacob et al., 2004; Sobrino et al., 2008), surface emissivity of forest canopy (esur), however, is generally above 0.9 (Hewison, 2001; Male and Granger, 1981; Seyednasrollah and Kumar, 2013; Wilber et al., 1999). H depends on the air convective coefficient and surface-air temperature difference, $\Delta T = TS - TA$ (i.e. $H \propto \Delta T$). SI can be directly measured, but LI, LO and H are more difficult to obtain at large scales and are often underestimated (Leuning and Foster, 1990; Nagler et al., 2003). In most studies, H is estimated using the Bowen ratio (e.g. Kalthoff et al. (2006)) or empirical canopy resistance (Lagos et al., 2013). Net thermal flux (i.e. LI - LO) is often approximated solely on the basis of air temperature, resulting in significant errors (Leuning and Foster, 1990; Nagler et al., 2003). Penman (1948) and Monteith (1964) were the first to use the energy balance approach to fully parametrize evapotranspiration from a vegetated surface. However, their model requires extensive meteorological data and calibration. The Penman-Monteith model was later simplified by Priestley and Taylor (1972) and Stone and Horton (1974), who neglected either H or R. This simplification decreases model accuracy when H or R are of the same order of magnitude (Ham et al., 1990; Jarvis and McNaughton, 1986;

Lagos et al., 2013).

Accounting for evaporative cooling can improve estimates of H and hence canopy water use. For a given net radiation, the heat loss from increasing ET is balanced by declining H and, thus, in thermal stress, known as the "cooling effect". Although the cooling effect of evapotranspiration has been studied in recent years (Ding et al., 2013; Mildrexler et al., 2011a, b; Yang et al., 2013), the effect has not yet been fully quantified at large regional scales and with seasonal variations. A qualitative comparison of the ΔT map with the seasonally averaged NDVI (see Fig. S1 of the Supporting information) suggests how vegetation distribution affects energy balance at the surface. Seasonally averaged ΔT declines with increasing vegetation indices for all land cover types. High vegetation cover and high evapotranspiration coincides with the lowest ΔT , resulting in sharp changes in ΔT at changes in vegetation cover. Although, surface albedo and thermal emissivity may vary across regions, these strong patterns of ΔT are mainly related to changes in the evaporative heat loss. In areas with negligible evapotranspiration due to the lack of water, plants, or both, the incoming energy received as solar radiation is accumulated at the surface (Mildrexler et al., 2011a), causing ΔT to increase. Similarly, water-use results in the cooling effect. The magnitude is mainly determined by a) varying convective heat transfer through variation in wind speed (Gates, 1966), relative humidity (Gates, 1968), stomatal control of leafwater loss (Drake et al., 1970; Jones, 2013), leaf orientation (Clum, 1926), and leaf size (Geller and Smith, 1982); and b) variation in sensible heat with varying insolation and air temperature (Pallas and Harris, 1964).

Quantifying the variability of ΔT with evapotranspiration under different conditions is needed to determine whether or not thermal stress can be used for monitoring drought across climates and regions (Anderson et al., 2007; Norman et al., 1995; Seguin and Itier, 1983). Previous remote sensing efforts have used canopy temperature (Norman et al., 2016), or cumulative degree days as indirect waterstress indices (Jackson et al., 1977), requiring extensive site-specific (Maeda et al., 2011) and climate-specific (Kalma et al., 2008) calibration efforts. We hypothesized that direct use of ΔT in the surface energy balance (Bausch et al., 2011; Bright et al., 2017) might bring more information on soil water status and stomatal conductance than is available from conventional indices (Faver et al., 1989). If so, then surface energy balance that predicts eddy-flux evapotranspiration data from satellite data should improve drought-stress predictions, and a spatiotemporal sensitivity analysis is critical.

This study presents a simple stochastic method based on surface energy balance to predict evapotranspiration from remote sensing over a wide range of atmospheric-demand and soil-moisture conditions. Our model allows us to predict the spatial and temporal variability of evapotranspiration with remotely sensed surface-air temperature difference. We combine a physical model with remotely sensed data and a Bayesian hierarchical model to estimate daily evapotranspiration at the scale of a forest stand to the subcontinent. Our approach is unique in accommodating uncertainties and requiring minimal satellite observation data to rapidly quantify surface water balance. Using space-borne surface temperature, we demonstrate how forest thermal stress - defined as surface-air temperature difference - allows us to monitor drought at the continental scale, using the example of the contiguous United States over the past 15 years. We use field data of evapotranspiration from sites across the southeastern and northwestern United States to validate the model.

2. Material and methods

If space-based estimates are to provide estimates of drought stress, they must predict synchronized evapotranspiration estimates from the ground-based eddy flux data spanning a range of forest types. We combine a physical model with remotely sensed data and a Bayesian hierarchical model to estimate daily evapotranspiration in forest stands

	etudy citee
	information
Table 1	Coognaphical information etudy eites

Geographical information study sites.	y sites.			
Site / ID	Ecoregion	Forest type	Lat./Lon./ Elev.	Citation
Chestnut Ridge / ChR	Valley and Ridge, TN, USA	Deciduous Broadleaf	35.93°/ -84.33°/ 290 m	(Meyers, 2005)
Duke Hardwoods / Dk2	Piedmont, NC, USA	Deciduous Broadleaf	35.97°/ -79.10°/ 168 m	(Oishi et al., 2001-2008aOishi et al., 2001-2008a)
Duke Loblolly/ Dk3	Piedmont, NC, USA	Evergreen Needleleaf ("75%) / Deciduous Broadleaf ("25%)	35.98°/-79.09°/ 169 m	(Oishi et al., 2001-2008bOishi et al., 2001-2008b)
Mary's River (Fir) / MRf	Pacific Border, OR, USA	Evergreen Needleleaf	44.65°/ -123.55°/ 265 m	(Law, 2005)
Loblolly Plantation / NC2	Coastal Plain, NC, USA	Evergreen (Loblolly Pine)	35.80°/ -76.67°/ 5 m	(Noormets, 2005)

as basis for subcontinent-scale analysis. Our model is physically consistent, probabilistically coherent, and can be implemented at large spatial extents (Wardlow et al., 2016). The study consists of two parts, a) *Inference*: modeling evapotranspiration from field and satellite observations at the stand scale, and b) *Comparison*: synthesizing thermal stress anomalies and its sensitivity for drought monitoring at the continental scale and its comparison with conventional drought indices.

The primary analysis is based on in-situ measurements of climate variables, evapotranspiration, and remotely sensed surface temperature at five contrasting forest sites in the USA (see Table 1). The sites include a wide range of climate and physiographic conditions with varying species compositions. See Fig. S2 for the boundaries of physiographic provinces. Climate data, including solar radiation, air temperature, and wind speed, were obtained from in-situ measurements and the Ameri-Flux dataset (https://fluxnet.ornl.gov). In the second part, we mapped thermal stress anomalies across the USA for fifteen years and compare it with conventional drought indices.

2.1. Data

Data for the model and the inter-comparison sections are presented in Tables S1 and S2, respectively. Site selection was based on three criteria: 1) availability of evapotranspiration and meteorological data including air temperature, solar radiation, thermal radiation, and wind speed, 2) continuous forest canopy coverage for at least an area larger than the size of 3×3 MODIS pixels to justify the usage of surface temperature as canopy temperature, and 3) excluding young stands and low-density forests. Study sites are distributed in the northwestern and southeastern USA (Table 1). Evapotranspiration and meteorological data used to fit the model were collected from flux towers using the eddy-covariance technique. Canopy temperature data were obtained from land surface temperature (MOD11A1, daily, 1 km resolution) from NASA's Moderate Resolution Imaging Spectroradiometer (MODIS) (DAAC, 2015). Satellite measurements of surface temperature were synchronized with the hourly evapotranspiration and air temperature data. For this integration with satellite data, mid-day measurements of evapotranspiration were used to summarize variation of daily average evapotranspiration (Gupta and Saxena, 1976) and to coincide with the timing of satellite imagery (approximately between 11:30 to 13:30, everyday).

Data used in the continental synthesis of drought stress were obtained from publicly available datasets, with full coverage of the continental USA. Surface temperature data from MODIS MOD11C1 (global, 0.05° resolution) are available since the year 2000. Temporal and normal air temperature data were obtained from PRISM Climate Data at 800-m resolution (PRISM, 2004). Radiation values were calculated from cloud cover data as explained in Appendix A. Cloud cover data from the Global Cloud Cover dataset (http://www.earthenv.org/cloud) incorporate 15 years of twice-daily cloud cover observations at 1000 m resolution (Wilson and Jetz, 2016). Land cover data were obtained from the National Land Cover Database 2011 (Homer et al., 2015) from Multi-Resolution Land Characteristics Consortium (MRLC). Monthly NDVI data were acquired from MODIS product MOD13 C3. Drought indices are obtained from multiple sources listed in Table S2.

Drought indices to compare against thermal stress anomalies were obtained from publicly available datasets. The terrestrial evapotranspiration index (ET) was collected from the MODIS Global Evapotranspiration Project. Soil moisture (SM) data were collected from the Climate Prediction Center of NOAA. The Global Terrestrial Drought Severity Index (DSI) was collected from Numerical Terradynamic Simulation Group. The Standardized Precipitation Index (SPI) was obtained from the National Center for Atmospheric Research (NCAR). The Standardized Precipitation-Evapotranspiration Index (SPEI) was obtained from the Spanish National Research Council (CSIC). The Palmer Drought Severity Index (PDSI) was obtained from the University Corporation for Atmospheric Research (UCAR). All data

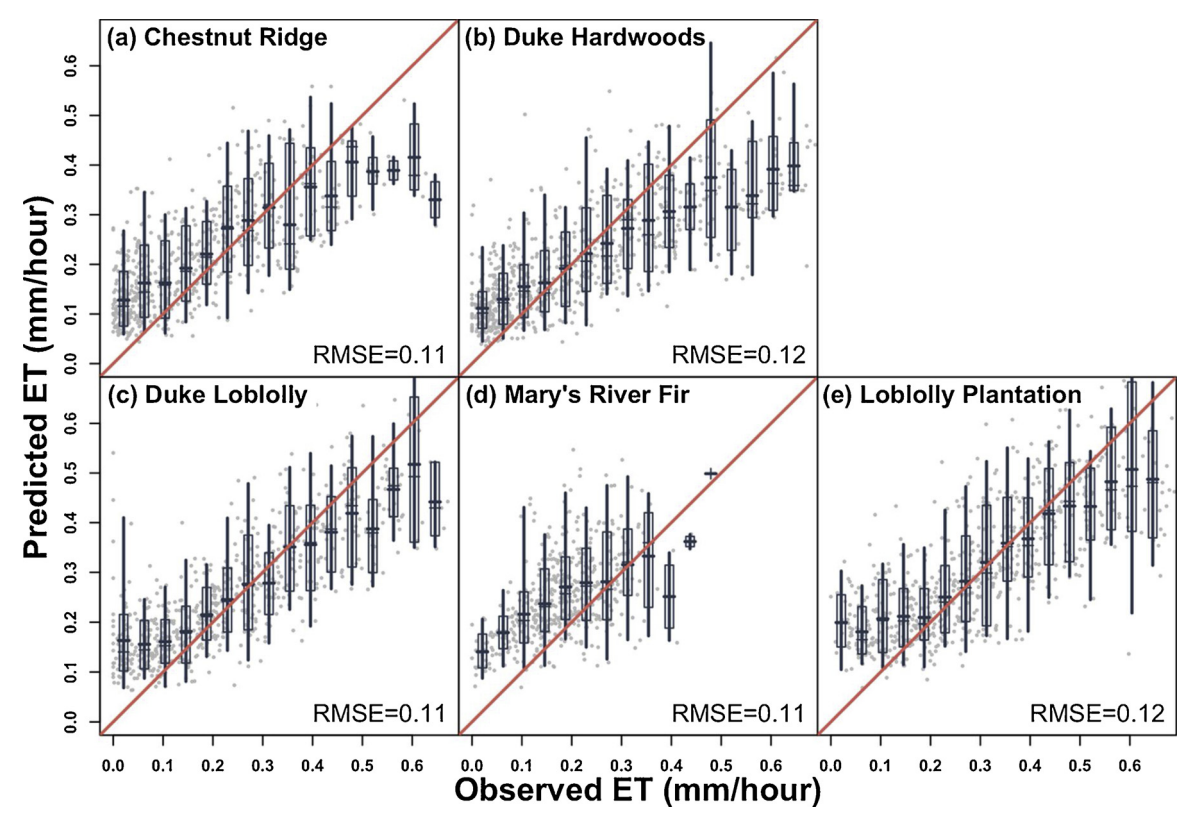


Fig. 1. Comparison of predicted vs. observed evapotranspiration flux per site for out-of-sample data. Evapotranspiration at each site is predicted based on a fitted model on all the other sites. For each graph, the gray dots are measured mid-day evapotranspiration data. The boxes and whiskers indicate 50% and 95% of the predictive interval. The red solid line indicates the 1:1 relationship. (For interpretation of the references to colour in this figure legend, the reader is referred to the web version of this article).

were obtained for the summer season (July to September) across the US. Sources of data are shown in Table S2.

2.2. Evapotranspiration model

A process-based model was developed to infer and predict evapotranspiration from the energy-balance. The data obtained from five study sites across the continental USA were used in the model. All data were used in a consolidated model where the model parameters are site-specific. The average model was fitted with parameters that were not site specific. Predicted evapotranspiration data for each site were obtained by leave-one-out cross-validation method. We repeated this procedure for all the study sites to avoid site-specific biases. Based on the energy conservation law, evapotranspiration depends on solar radiation, thermal radiation, and sensible heat. The ground heat flux is assumed to be proportional to solar radiation (Choudhury et al., 1987). ET (mm/day) data from eddy flux sites can be described by a Bayesian model, censored at zero, and a Gaussian error (τ^2), having likelihood

$$ET_{s,t} \sim N(\mu_{s,t}, \tau_s^2)$$

$$\mu_{s,t} = \frac{R_{s,t} + LI_{s,t} - LO_{s,t} - H_{s,t}}{\lambda}$$

where $N(\mu, \tau^2)$ is the normal distribution with mean (μ) and standard deviation (τ) values. s and t are site and time indices. λ is the latent heat of vaporization and relates to air temperature (TA) as $\lambda = 2502 - 2.308 \, TA$ in J. g⁻¹. Energy fluxes can be obtained from:

$$R_{s,t} = \alpha_s SI_{s,t}$$

$$LI_{s,t} = \sigma \varepsilon sur_s TA_{s,t}^4$$

$$LO_{s,t} = \sigma \varepsilon sky_s TS_{s,t}^4$$

$$H_{s,t} = h_{s,t} \Delta T_{s,t}$$

$$h_{s,t} = c_s W_{s,t}^{a_s}$$

$$\Delta T_{s,t} = TS_{s,t} - TA_{s,t}$$

where α_s is the solar absorption coefficient for site s. σ is the Stefan-Boltzmann constant and $\sigma=5.67\times10^{-8}Wm^{-2}K^{-4}$. εsky_s and εsur_s are emissivity coefficients for sky and surface at site s, respectively. TS and TA are surface and air temperatures, respectively. W is wind speed (m/s). h is the convective heat transfer coefficient (Wm $^{-2}K^{-1}$). a and c terms are constants for the convective heat transfer. The prior distributions of the parameters are assumed to be uniform within the physically valid ranges:

$$\sigma_s^2 \sim IG(0.1, 0.1)$$

$$\alpha_s \in [0, 1]$$

 $\varepsilon sky_s \in [0.60, 0.85]$

 $\varepsilon sur_s \in [0.90, 0.99]$

 $c_s \in [0, \infty)$

$$a_s \in [0.5, 0.8]$$

where IG denotes the inverse gamma distribution. Gibbs sampling (Markov chain Monte Carlo) was implemented for posterior distributions of all the parameters. Sensitivity time-series and maps were generated for the derivative of the fitted model with respect to ΔT and TS. Assuming $\frac{\partial TA}{\partial \Delta T} = -1$, $\frac{\partial TS}{\partial \Delta T} = +1$, and $\frac{\partial (1/\lambda)}{\partial TA} \approx 0$, the sensitivity values of evapotranspiration to ΔT , and TS are obtained from:

$$\left(\frac{\partial ET}{\partial \Delta T}\right)_{s,t} = -\frac{1}{\lambda}$$
. (4. σ . $\varepsilon s k y_s$. $T A_{s,t}^3 + 4$. σ . $\varepsilon s u y_s$. $T S_{s,t}^3 + h_{s,t}$)

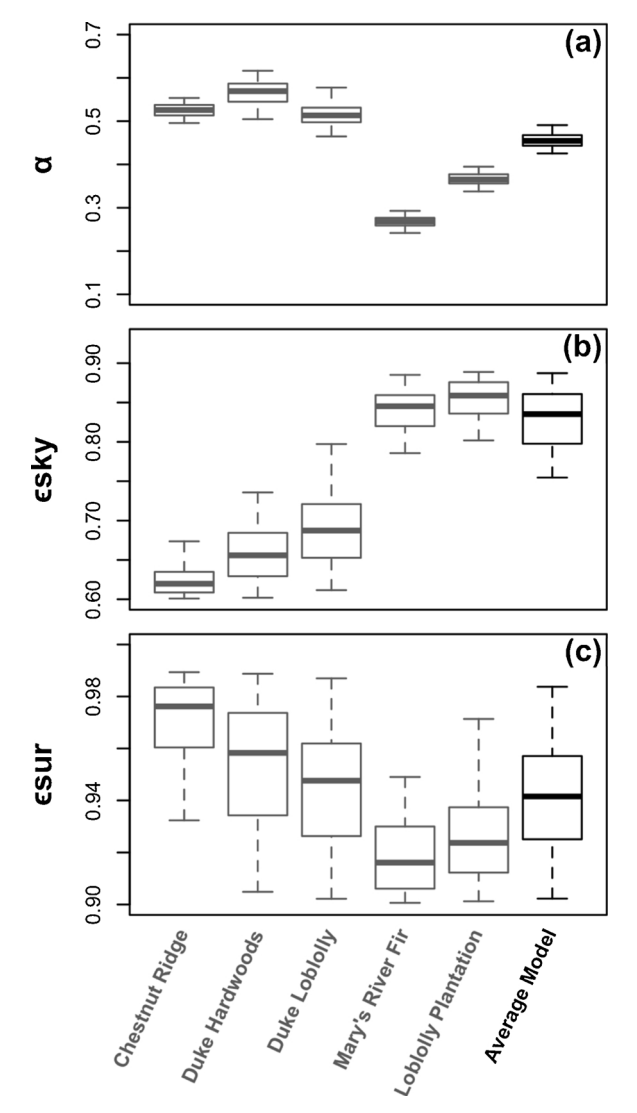


Fig. 2. Posterior distributions of the model parameters when fitted to each site independently and for all sites in combination.

and

$$\left(\frac{\partial ET}{\partial TS}\right)_{s,t} = -\frac{1}{\lambda}.$$
 (4. $\sigma. \ \epsilon sur_s. \ TS_{s,t}^3 + h_{s,t}$)

For the second part of the study, inter-annual anomalies in ΔT were compared with inter-annual anomalies in soil moisture and evapotranspiration from climate and weather prediction models. These anomalies values were obtained as the difference between temporal data and historical monthly averages.

3. Results

Cross validations of the model at the study sites showed predicted evapotranspiration (ET) data are reliable across a broad range of soil and climate conditions (Fig. 1). The posterior distribution shows differences and similarities across sites (Fig. 2). Low solar absorption (α) at the Mary's River Fir site is explained by a partial clear-cut that increased surface albedo. Duke Hardwoods, Duke Loblolly, and Chestnut Ridge showed slightly higher α than the Loblolly Plantation site, where canopy coverage is sparse. We did not expect sky and surface emissivity coefficients (εsky and εsur) to agree between sites, due to differences in cloud cover (controlling εsky) and species composition (controlling εsur) across sites. Low εsky estimates for Duke Hardwood, Duke

Loblolly, and Chestnut Ridge sites were expected due to lower cloud cover compared to Mary's River Fir and Loblolly Plantation sites (Fig. 2-b). Variation in εsur spans the expected range of 0.9–1 across sites. The values of εsur were somewhat above the average for Duke Hardwood and Chestnut Ridge sites, which are dominated by deciduous species (Fig. 2-c). Mary's River Fir and Loblolly Plantation sites showed slightly lower εsur where evergreens are abundant (almost pure evergreen). Although the Duke Loblolly is also mainly evergreen (~75%), the MODIS pixel used to extract surface temperature data partially overlaps with an adjacent mixed deciduous forest, explaining the intermediate εsur value.

All four energy components (i.e. solar, incoming and outgoing thermal radiations and sensible heat) make considerable contributions to variation in evapotranspiration, indicating the importance of each term for estimating ET (Fig. S3). Although, sensible heat is lower than the other three fluxes, it still makes a significant contribution to the energy balance.

The total effect of ΔT varies seasonally with wind speed and surface and air temperatures. ET increases with decreasing ΔT or TS and with increasing TA. A sensitivity analysis of ΔT and surface temperature effects over a typical year (with historical average seasonal variations) at five studied sites (Fig. 3) showed that the ΔT effect is weakest (least negative) during the cold season (approximately days 1–20 and 340–365). With increasing temperature in spring, a 1 °C change in the ΔT can potentially relate to 1–1.25 mm day $^{-1}$ changes in evapotranspiration (variation of sensitivity in Fig. 3). During late spring and early summer (after day 170), the ΔT and surface temperature controls continue to increase, as solar radiation decreases, but temperature continues to rise. This trend persists until the onset of cooling in autumn (after day 210), and then gradually becomes less negative until the end of the year. Despite difference between sites' climates and ecosystems, the sensitivity trends were similar across sites.

Thermal stress sensitivity varies with climate and between ecoregions. Based on the historical average of air and surface temperature, we quantified variability of summer (July, August and September) ET with ΔT and surface temperature (TS) across the USA conditional on a continuous forest cover (Fig. 4). Spatiotemporal variation of ET with ΔT is driven by variation in air and surface temperature (Fig. 4-a). ΔT sensitivity is highest (most negative) in northern plateaus and across the southern regions, and lowest in cool areas of the north and mountainous regions. The overall spatial thermal stress sensitivity varies from 1.1 to 1.2 mm/day/°C. Sensitivity of ET to TS is everywhere negative, but also varies regionally (Fig. 4-b).

To identify regions with severe drought, satellite observation of surface temperature and assimilated air temperature data were used to quantify thermal stress anomalies over the last 15 years (ΔT in Fig. 5). For example, the results for 2007 show considerable thermal stress anomalies not only in much of the western US, but also in northern areas of northeastern US and parts of the southeastern Coastal Plain.

Anomaly values of ΔT were compared with anomalies of several indices and metrics including the terrestrial *evapotranspiration (ET, MODIS)*, soil moisture (*SM, NOAA*), drought severity index (*DSI, MODSI*), the Standardized Precipitation Index (*SPI, NCAR*), the Standardized Precipitation-Evapotranspiration Index (*SPEI, CSIC*), and the Palmer Drought Severity Index (*PDSI, UCAR*). Since all of these quantities are commonly used for drought monitoring, they should agree on the general patterns of severe water shortage across the regions. However, site-to-site correlations with one another never rise to the level of 0.5 (except for the correlation between similar indices SPI and SPEI; see Fig. 6). By contrast, all correlations with ΔT exceed 0.5. Finally, ΔT is more highly correlated with evapotranspiration from MODIS (ET) and soil moisture from NOAA (SM) than are any metrics currently in use for drought monitoring (Fig. 6).

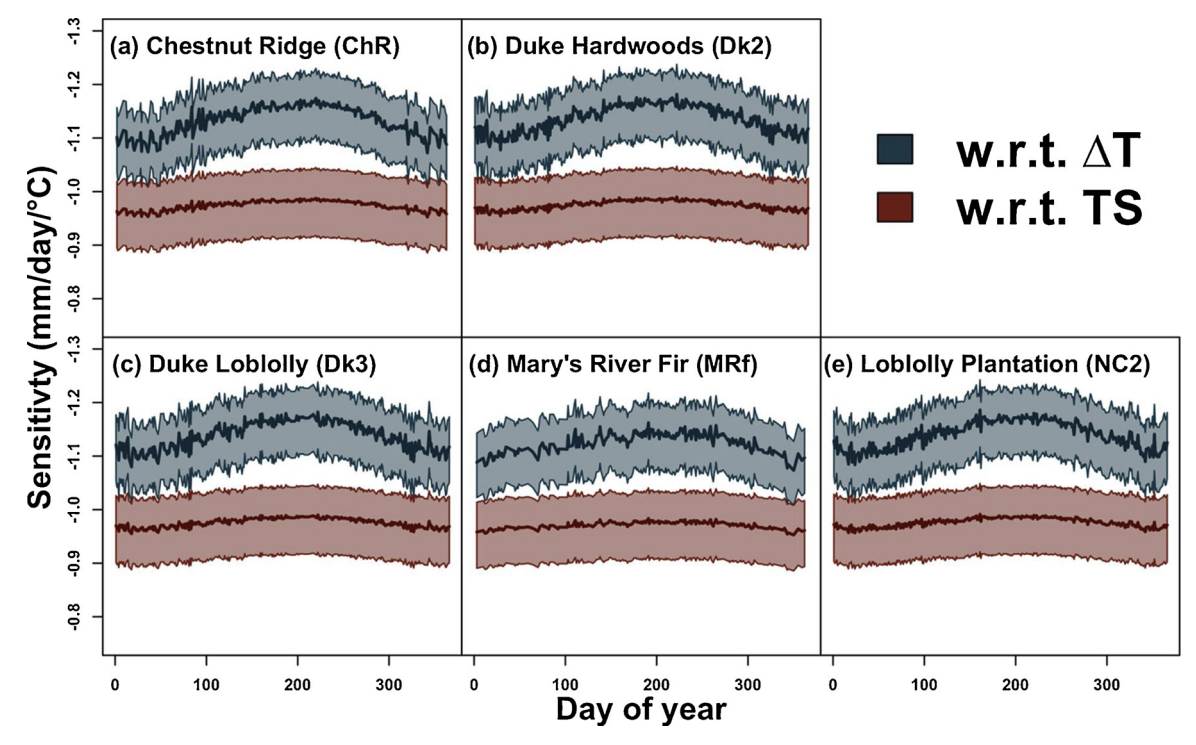


Fig. 3. Seasonal variation of sensitivity of evapotranspiration with respect to thermal stress (ΔT) and surface temperature (TS) at the five study sites. Shaded areas are 95% predictive intervals. The ΔT effect remains strong throughout summer when monitoring drought is most important. Note the inverted y axis.

4. Discussion

Remotely sensed surface-air temperature difference (ΔT) allowed us to identify water stressed regions from energy balance relationships and with more accuracy than conventional drought indices such as soil moisture anomalies, DSI, or PDSI. This was evident by comparing the sum of one-to-one correlation values between all of the studied metrics. The ΔT anomaly is a strong indicator of drought, particularly in warm and dry seasons and regions, i.e., the times and places drought monitoring is needed most. In addition, unlike many remotely sensed approaches that use near infra-red and thermal infra-red bands (Kustas and Anderson, 2009), vegetation indices or gross primary productivity to estimate evapotranspiration (Hilker et al., 2013; Price, 1982; Yang et al., 2013), this method is physically consistent and can be implemented at large spatial extents. Our ground-based analysis of evapotranspiration validated the thermal stress and showed how energy fluxes compare in terms of their contributions to evapotranspiration and allowed for extensive sensitivity analyses.

As we expected, results showed that all energy flux terms, including net solar and thermal radiation and sensible heat, contributed to surface energy balance with comparable magnitudes (Fig. S3). The effects of energy components vary across regional climate gradients and site physical properties, including α , εsur and εsky . Slightly stronger absorption of solar radiation at deciduous sites Duke Hardwood and Chestnut Ridge than mainly evergreen sites Loblolly Plantation and Mary's River Fir are explained by differences in surface albedo (Chapin et al., 2011; Hollinger et al., 2010), vegetation density and ground heat flux across sites (Fig. 2-a).

Sky cloudiness, surface emissivity, and surface and air temperatures are the most important influences on net thermal radiation. The net effects of thermal radiation on evapotranspiration may depend on several factors. Thermal radiation consists of two main components, the incoming thermal energy from the surrounding atmosphere (LI) and the emitting thermal energy from canopy surface (LO). The incoming thermal energy (LI) is proportional to TA^4 and sky emissivity coefficient (esky). The emitting thermal energy (LO) varies with TS^4 and the

surface emissivity coefficient (εsur). While εsky may vary with atmospheric conditions and cloud cover, εsur does not. With increasing cloud cover, εsky increases. Therefore, regions with fewer days of clear sky conditions may experience a large effect of thermal radiation on evapotranspiration and surface energy balance. If so, then the coastal sites may experience a larger εsky and LI effect on evapotranspiration than do sites in the Piedmont and the Valley and Ridge (Fig. 2-b). Slight differences in εsur across sites may be related to surface emissivity of evergreen and deciduous species. LO may play a stronger role in surface energy balance on sites that are dominated by species with high thermal emissivity.

We demonstrated that evapotranspiration decreases with thermal stress and surface temperature through sensible heat and the emitting thermal radiation (Fig. 3). By quantifying uncertainty in the Bayesian model, we showed that the magnitude of the ΔT effect is comparable to the effects of solar radiation and air temperature. The ΔT effect results as sensible heat (H), the convective energy transfer from the leaf surface. H depends on the surface-air temperature difference, wind speed, thermal conductivity, and heat capacity of the surrounding air. The ΔT effect is amplified in windy days as convective heat transfer increases. As wind speed increases, air flow becomes turbulent, increasing sensible heat (Maes and Steppe, 2012) and, thus, the ΔT effect on windy days and in regions where windy weather is common. An amplifying effect of ΔT with increasing air temperature and decreasing solar radiation is understood from the contribution of sensible heat to surface energy balance relative to that of solar radiation. The ΔT effect varies seasonally, as it interacts with changing air and surface temperatures (Fig. 3). The highest sensitivity of surface energy balance to ΔT occurs in late summer, when it is most needed to monitor droughts.

Variability of evapotranspiration with ΔT varies regionally (Fig. 4), mainly caused by differences in climate and surface temperature. Low temperatures in the north and at high elevations result in low ΔT sensitivity. High cloud cover and northern latitudes receive low net solar radiation, thus amplifying the relative ΔT effect. Our results indicated that thermal stress may account for evapotranspiration variation in the range from 1.0 to 1.25 mm/day/°C (Figs. 3 and 4). In other words,

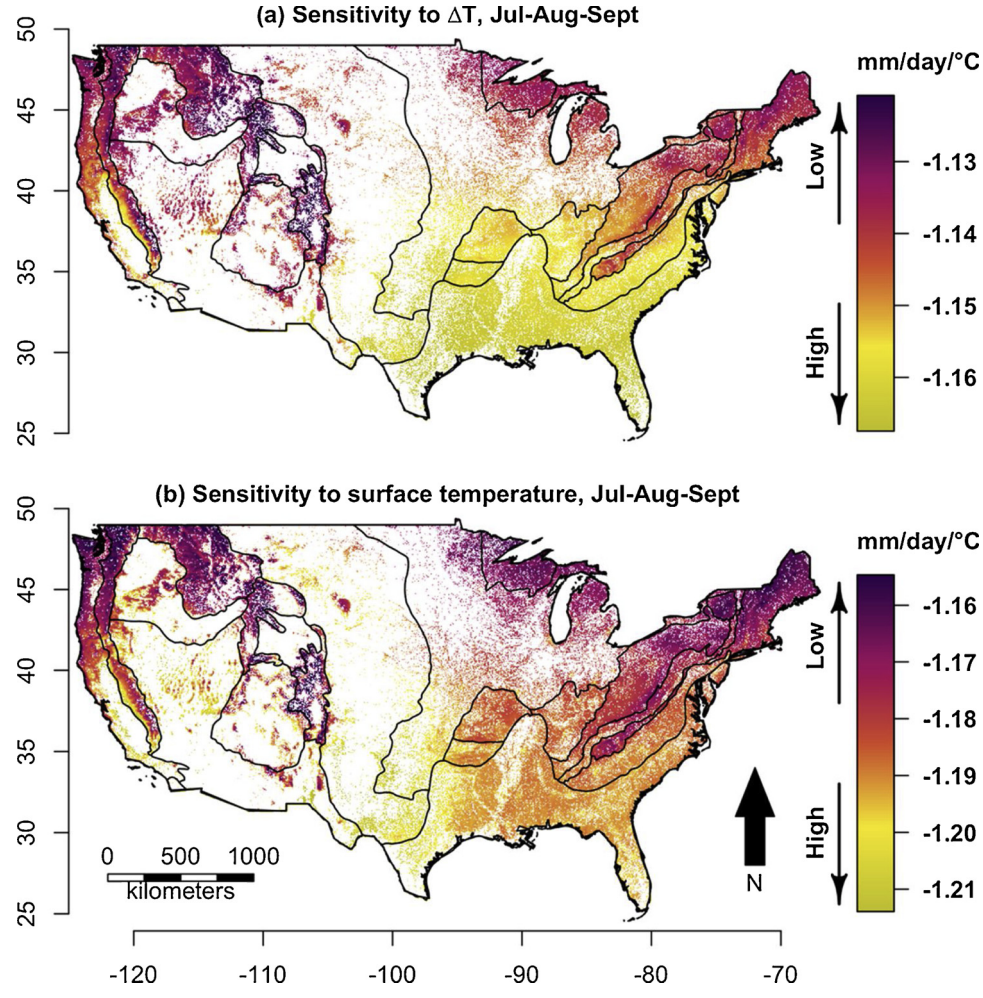


Fig. 4. Geographic sensitivity of evapotranspiration to (a) ΔT , and (b) TS in the United States. The ΔT effect is highest in warmer regions, southern sites, coastal areas, and low- to mid-latitude plateaus. Solid black lines indicate the boundaries of physiographic provinces (see Figure S2 for the boundaries of physiographic provinces). The yellow color indicates high (more negative) ΔT or TS sensitivity. Areas with no tree coverage are shown in the white color. (For interpretation of the references to colour in this figure legend, the reader is referred to the web version of this article).

1 mm/day of evapotranspiration may contribute a "cooling effect" of 0.8 to 1 °C. This is lower than the estimates for croplands (Pallas and Harris, 1964; Tew, 1962) and forests (Ballinas and Barradas, 2016; Rahman et al., 2017) in previous studies. The effect is largest near coastlines and in the south where temperature is high.

Remotely sensed thermal stress showed the strongest correlation with conventional drought indices (Figs. 5 and 6). The fact that thermal stress was able to identify regions of drought severity across the entire United States demonstrated how integrating ΔT anomalies, calibrated with measured evapotranspiration data from multiple locations, can improve monitoring. ΔT anomalies and evapotranspiration anomalies need not be equal, but rather, proportional to each other in the energybalance model at the times when evapotranspiration is occurring (Fig. 6). An extended mathematical description of the ΔT -ET relationship is detailed in Appendix B. Given this proportionality, ΔT alone is sufficient as a near-real-time drought monitor, whereas the model is needed to translate ΔT to evapotranspiration anomalies. The high correlation values ΔT anomalies with conventional drought metrics showed that ΔT anomaly can be used as a single indicator of drought when solar radiation data are lacking. This effect becomes even more important in regions with stable year-to-year solar radiation (negligible radiation anomalies) and warming climates (high surface and air temperature anomalies).

 ΔT anomalies can be used for instantaneous and long-term monitoring of drought at coarse spatial scales (Inoue et al., 1994). We have

implemented a live interface that visualizes monthly thermal stress as well as its monthly anomalies and normal variables for the contiguous United States in near real-time. The interface can be access online via https://bnasr.github.io/droughteye/. The interface will be automatically updated as new satellite data become available on a monthly basis. The data are also publicly available for download through the same interface. The code is available from Seyednasrollah (2018).

5. Conclusions

We demonstrated how remotely sensed thermal stress anomaly can be used as a simple but reliable metric for near real-time monitoring of drought at large spatial extents. Our sensitivity results showed that thermal stress has the strongest relationship with evapotranspiration in warm regions and seasons, where and when monitoring drought is most critical. We presented a live implementation of thermal stress across the contiguous United States that enables drought monitoring in near real-time.

While thermal stress anomalies can be used as a single metric for water stress, the accuracy in predicting forest water use may improve with remotely sensed vegetation density estimates and surface physical properties such as albedo and emissivity, and with increased spatial resolution. Current global satellite–based surface temperature data that include up to 1.4 °C measurement error (Sanchez et al., 2007) can be improved with high resolution surface temperature data (Nagler et al.,

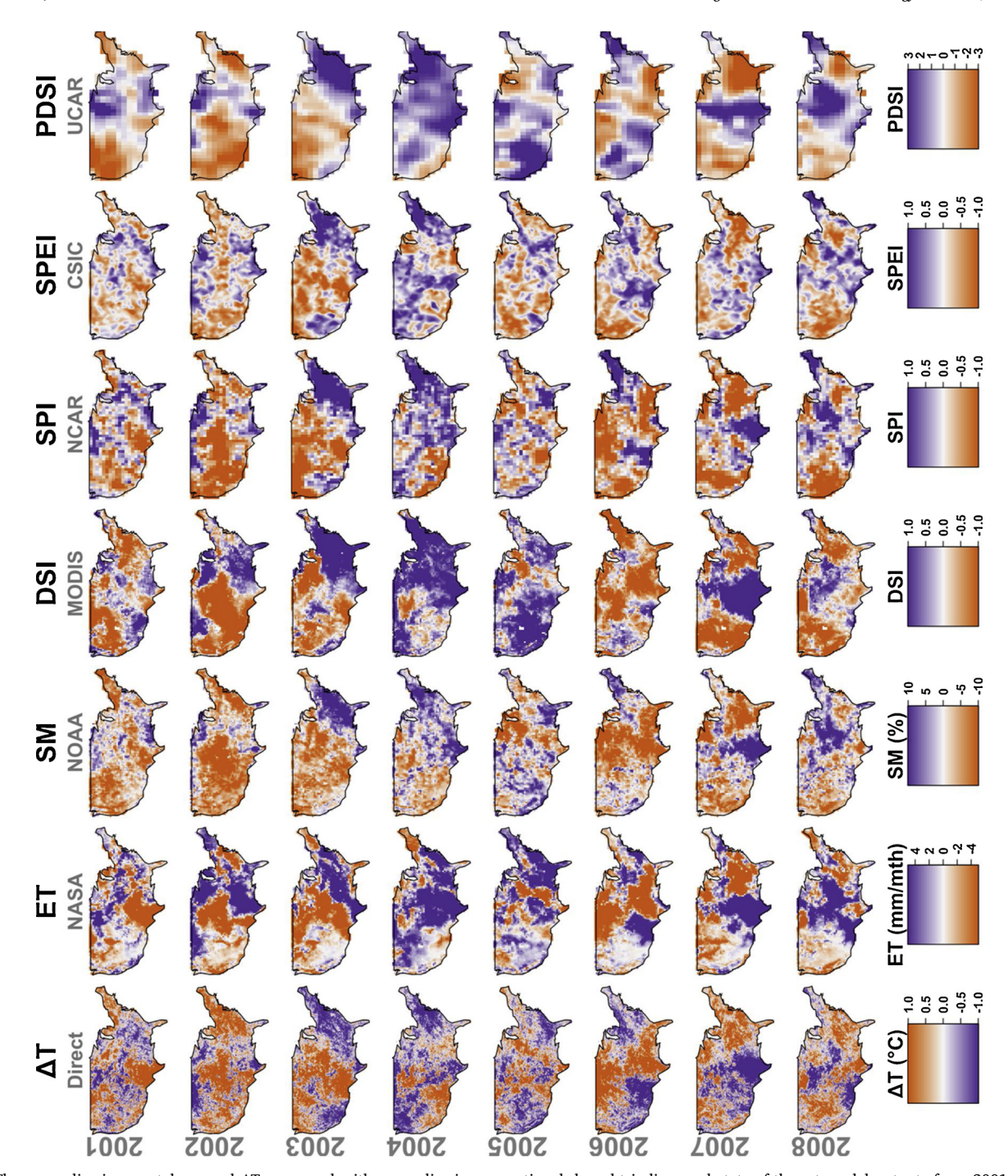


Fig. 5. The anomalies in remotely sensed ΔT compared with anomalies in conventional drought indices and state-of-the-art model outputs from 2001-2008. ΔT anomaly identifies regions with high water stress. Acronyms are ET = evapotranspiration anomaly, SM = soil moisture anomaly, DSI = Drought Severity Index, SPI = Standardized Precipitation Index, SPEI = Standardized Precipitation-Evapotranspiration Index, and PDSI = The Palmer Drought Severity Index. Details about sources of data are explained in Table S2. A more comprehensive comparison for years 2001 to 2015 is presented in the supporting information.

2005). The results from this study in forest areas could modify parametrization techniques that estimate terrestrial energy balance of vegetation cover (Alkama and Cescatti, 2016), surface albedo, and evapotranspiration (Zhu and Zeng, 2015).

Acknowledgments

The project was funded by the Macrosystems Biology and Coweeta

LTER programs of the National Science Foundation (NSF-EF-1137364, NSF-EF-1550911). This research was also supported by a grant from the Duke Provost's Collaboratories initiative, and from the National Science Foundation (NSF-IOS-1754893). The evapotranspiration data were provided courtesy of the AmeriFlux sites: US-ChR, US-Dk2, US-Dk3, US-MRf, and US-NC2. The authors thank Chase Nunez and Bradley Tomasek for their constructive comments on the manuscript.

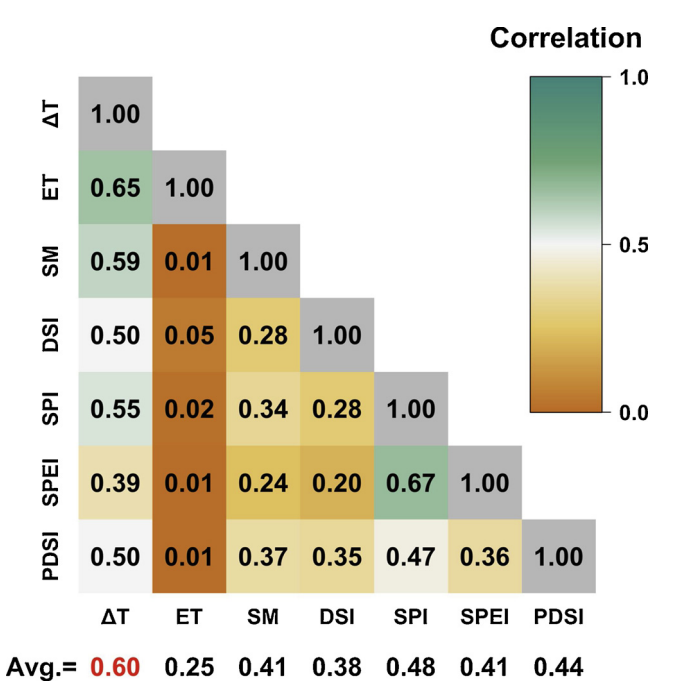


Fig. 6. Correlation values between thermal stress anomalies and conventional drought indices and predicted evapotranspiration (ET). Average correlation values are shown for each index. ΔT shows the highest average correlation with all other metrics. Acronyms for the drought indices are SM = soil moisture anomaly, DSI = Drought Severity Index, SPI = Standardized Precipitation Index, SPEI = Standardized Precipitation-Evapotranspiration Index, and PDSI = The Palmer Drought Severity Index.

Appendix A. Calculation of solar radiation

Incoming solar radiation is calculated as:

$$I_s = G_t. (1 - 0.75. C_{s,t}^3). \cos(\psi_{s,t})$$

where the subscripts s and t indicate site and time, respectively. I is the incoming solar radiation, G is top of the atmosphere solar radiation, C is the cloud coverage, and ψ is the solar zenith angle (Seyednasrollah and Kumar, 2014; Seyednasrollah et al., 2013). G for the N'th day of year is evaluated from (Kalogirou, 2009):

$$G_t = K. \left[1 + 0.033 \cdot \cos\left(\frac{360 \, D}{365}\right) \right]$$

where $K = 1366.1 W/m^2$ is solar constant and D is the day of year. ψ is approximated by solving:

$$cos(\psi_{s,t}) = sin(L_s). sin(\delta_t) + cos(L_s). cos(\delta_t). cos(15^{\circ}. (AST - 12))$$

where L is the site latitude, δ_t is solar declination angle (in degree), $\delta_t = 23.45^{\circ} sin\left(\frac{360}{365}(284 + D)\right)$, and AST is the apparent solar time (in hours).

Appendix B. Near-unity correlation between ET anomalies and ΔT anomalies

The daily anomalies can be written as

$$\lambda. \ \delta ET = \delta R + \delta LI - \delta LO - \delta H \tag{1}$$

where anomaly δ indicates the inter-annual deviation from the historical mean on a given day. Upon substituting for LI, LO and H terms (see main text), we obtain:

$$\lambda$$
. $\delta ET = \delta R + \sigma \varepsilon sky \delta(TA^4) - \sigma \varepsilon sur \delta(TS^4) - h \delta(\Delta T)$

Assuming solar radiation anomalies are negligible, $\delta R \approx 0$ and $TA = TS - \Delta T$, we have

$$\lambda$$
. $\delta ET = \sigma \varepsilon sky \delta((TS - \Delta T)^4) - \sigma \varepsilon sur \delta(TS^4) - h \delta(\Delta T)$

which expands to:

$$\lambda. \ \delta ET = \sigma \ \varepsilon sky \ \delta (TS^4 - 4.TS^3. \ \Delta T + 6. \ TS^2. \ \Delta T^2 - 4. \ TS. \ \Delta T^3 + \Delta T^4) - \sigma \ \varepsilon sur \ \delta (TS^4) - h. \ \delta (\Delta T)$$
 (2)

Replacing

$$\delta(TS^4) \approx 4. \ \bar{TS}^3. \ \delta TS$$

 $\delta(4. TS^3. \Delta T) \approx 4. T\bar{S}^3. \delta(\Delta T) + 12. T\bar{S}^2. \Delta T. \delta TS$

 $\delta(6. TS^2. \Delta T^2) \approx 12. \overline{TS}^2. \Delta \overline{T}. \delta(\Delta T) + 12. \overline{TS}. \overline{\Delta T}^2. \delta TS$

 $\delta(4.\ TS.\ \Delta T^3) \approx 12.\ \overline{TS}.\ \Delta T^2.\ \delta(\Delta T) + 4.\ \Delta T^3.\ \delta TS$

$$\delta(\Delta T^4) \approx 4. \ \Delta T^3. \ \delta(\Delta T)$$

where bar indicates annual average values, we rewrite Eq. (2) as:

 $\lambda.~\delta ET \approx 4.~\sigma.~(\varepsilon s ky.~[\bar{T}S^3-3.~\bar{T}S^2.~\bar{\Delta T}+3.~\bar{T}S.~\bar{\Delta T}^2-\bar{\Delta T}^3] \\ -\varepsilon s ur.~\bar{T}S^3).~\delta TS~+(4.~\sigma.~\varepsilon s ky.~[-\bar{T}S^3+3.~\bar{T}S^2.~\bar{\Delta T}-3.~\bar{T}S.~\bar{\Delta T}^2+\bar{\Delta T}^3] \\ -h).~\delta(\Delta T) = -1.5$

Because $TS \gg \Delta T$ and, thus, $TS^3 \gg TS^2$. $\Delta T \gg TS \cdot \Delta T^2 \gg \Delta T^3$, low-order terms in the TS term disappear,

$$\lambda$$
. $\delta ET \approx 4$. σ . ($\varepsilon sky - \varepsilon sur$). \vec{TS}^3 . $\delta TS - (4$. σ . εsky . $\vec{TS}^3 + h$). $\delta (\Delta T)$

with the following comments on parameters and variables:

- σ is the Stefan-Boltzmann constant and equals $5.67 \times 10^{-8} Wm^{-2}K^{-4}$.
- Typical summer values for S may range from 300 K to 330 K and hence $T\bar{S}^3 \approx 3 \times 10^7$.
- εsur is between 0.9 to 0.98.
- ɛsky is between 0.6 to 0.9.
- \bullet h ranges from 5 to 30 W.m². K⁻¹

The above typical ranges show the $\delta(\Delta T)$ term in Eq. (3) is substantially larger than the δTS term, and proportional to ET, thus explaining the expected correlation between ET anomalies and ΔT anomalies.

Appendix C. Supplementary data

Supplementary material related to this article can be found, in the online version, at doi:https://doi.org/10.1016/j.agrformet.2019.02.016.

References

- Abbaszadeh, Peyman, Moradkhani, Hamid, Zhan, Xiwu, 2018. Downscaling SMAP radiometer soil moisture over the CONUS using an ensemble learning method. Water Resour. Res. https://doi.org/10.1029/2018WR023354.
- AghaKouchak, A., et al., 2015. Remote sensing of drought: progress, challenges and opportunities. Rev. Geophys. 53 (2), 452–480.
- Alkama, R., Cescatti, A., 2016. Biophysical climate impacts of recent changes in global forest cover. Science 351 (6273), 600–604.
- Allen, C.D., et al., 2010. A global overview of drought and heat-induced tree mortality reveals emerging climate change risks for forests. For. Ecol. Manag. 259 (4), 660–684.
- Allen, R., et al., 2011. Satellite-based ET estimation in agriculture using SEBAL and METRIC. Hydrol. Process. 25 (26), 4011–4027.
- Anderson, M.C., Norman, J.M., Mecikalski, J.R., Otkin, J.A., Kustas, W.P., 2007. A climatological study of evapotranspiration and moisture stress across the continental United States based on thermal remote sensing: 1. Model formulation. J. Geophys. Res. Atmos. 112 (D10).
- Anderson, M., et al., 2008. A thermal-based remote sensing technique for routine mapping of land-surface carbon, water and energy fluxes from field to regional scales. Remote Sens. Environ. 112 (12), 4227–4241.
- Badenas, C., 1998. Review and improvement of an algorithm for determining emissivity of a heterogeneous cavity in thermal infrared remote sensing. Int. J. Remote Sens. 19 (4), 731–741.
- Ballinas, M., Barradas, V.L., 2016. The urban tree as a tool to mitigate the urban heat island in Mexico city: a simple phenomenological model. J. Environ. Qual. 45 (1), 157–166.
- Bastiaanssen, W., et al., 1998a. A remote sensing surface energy balance algorithm for land (SEBAL).: part 2: validation. J. Hydrol. 212, 213–229.
- Bastiaanssen, W.G., Menenti, M., Feddes, R., Holtslag, A., 1998b. A remote sensing surface energy balance algorithm for land (SEBAL). 1. Formulation. J. Hydrol. 212, 198–212.
- Bastiaanssen, W., et al., 2005. SEBAL model with remotely sensed data to improve waterresources management under actual field conditions. J. Irrig. Drain. E 131 (1), 85–93.
- Bausch, W., Trout, T., Buchleiter, G., 2011. Evapotranspiration adjustments for deficitirrigated corn using canopy temperature: a concept. Irrig. Drain. 60 (5), 682–693. Beguería, S., 2017. sbeguería/SPEIbase: Version 2.5.1.
- Bright, R.M., et al., 2017. Local temperature response to land cover and management change driven by non-radiative processes. Nat. Clim. Change 7 (4), 296–302.
- Caselles, V., Coll, C., Valor, E., 1997. Land surface emissivity and temperature determination in the whole HAPEX-Sahel area from AVHRR data. Int. J. Remote Sens. 18 (5), 1009–1027.
- Chapin III, F.S., Matson, P.A., Vitousek, P., 2011. Principles of Terrestrial Ecosystem Ecology. Springer Science & Business Media.
- Chiesi, M., et al., 2013. Combination of ground and satellite data for the operational estimation of daily evapotranspiration. Eur. J. Remote Sens. 46, 675–688.
- Choudhury, B., Idso, S., Reginato, R., 1987. Analysis of an empirical model for soil heat

- flux under a growing wheat crop for estimating evaporation by an infrared-temperature based energy balance equation. Agric. For. Meteorol. 39 (4), 283–297.
- Clark, J.S., Vose, J.M., Luce, C.H., 2016. Forest drought as an emerging research priority. Glob. Change Biol. 22 (7) 2317-2317.
- Clum, H.H., 1926. The effect of transpiration and environmental factors on leaf temperatures II. Light intensity and the relation of transpiration to the thermal death point. Am. J. Bot. 13 (4), 217–230.
- Courault, D., Seguin, B., Olioso, A., 2005. Review on estimation of evapotranspiration from remote sensing data: from empirical to numerical modeling approaches. Irrig. Drain. Syst. 19 (3-4), 223–249.
- DAAC, N.L., 2015. Land surface temperature and emissivity daily L3 global 1 km grid SIN, MOD11A1. In: DAAC, N.L. (Ed.), NASA EOSDIS Land Processes DAAC. USGS Earth Resources Observation and Science (EROS) Center, Sioux Falls, South Dakota.
- Ding, R.S., Kang, S.Z., Li, F.S., Zhang, Y.Q., Tong, L., 2013. Evapotranspiration measurement and estimation using modified Priestley-Taylor model in an irrigated maize field with mulching. Agric. For. Meteorol. 168, 140–148.
- Drake, B.G., Raschke, K., Salisbury, F.B., 1970. Temperatures and transpiration resistances of Xanthium Leaves as affected by air temperature, humidity, and wind speed. Plant Physiol. 46 (2), 324-+.
- Faver, K.L., Otoole, J.C., Krieg, D.R., 1989. Short-term estimation of Sorghum evapotranspiration from canopy temperature. Agric. For. Meteorol. 48 (1-2), 175–183.
- Flerchinger, G., Xaio, W., Marks, D., Sauer, T., Yu, Q., 2009. Comparison of algorithms for incoming atmospheric long-wave radiation. Water Resour. Res. 45 (3).
- French, A., et al., 2005. Surface energy fluxes with the Advanced Spaceborne Thermal Emission and Reflection radiometer (ASTER) at the Iowa 2002 SMACEX site (USA). Remote Sens. Environ. 99 (1-2), 55-65.
- Gates, D.M., 1966. Transpiration and energy exchange. Q. Rev. Biol. 41 (4), 353-&. Gates, D.M., 1968. Transpiration and leaf temperature. Annu. Rev. Plant Physiol. 19, 211-&
- Geller, G.N., Smith, W.K., 1982. Influence of leaf size, orientation, and arrangement on temperature and transpiration in 3 high-elevation, large-leafed herbs. Oecologia 53 (2), 227–234.
- Guarín, A., Taylor, A.H., 2005. Drought triggered tree mortality in mixed conifer forests in Yosemite National Park, California, USA. For. Ecol. Manag. 218 (1), 229–244.
- Gupta, A., Saxena, M.C., 1976. Evaluation of leaf analysis as a guide to nitrogen and phosphorus fertilization of potato (Solanum-Tuberosum-L). Plant Soil 44 (3), 597–605.
- Ham, J.M., Heilman, J.L., Lascano, R.J., 1990. Determination of soil-water evaporation and transpiration from energy-balance and stem-flow measurements. Agric. For. Meteorol. 52 (3-4), 287–301.
- Hewison, T.J., 2001. Airborne measurements of forest and agricultural land surface emissivity at millimeter wavelengths. IEEE Trans. Geosci. Remote 39 (2), 393–400. Hilker, T., et al., 2013. Remote sensing of transpiration and heat fluxes using multi-angle
- observations. Remote Sens. Environ. 137, 31–42.
 Hollinger, D.Y., et al., 2010. Albedo estimates for land surface models and support for a
- Hollinger, D.Y., et al., 2010. Albedo estimates for land surface models and support for a new paradigm based on foliage nitrogen concentration. Glob. Change Biol. 16 (2), 606–710
- Homer, C., et al., 2015. Completion of the 2011 national land cover database for the

- Conterminous United States representing a decade of land cover change information. Photogramm. Eng. Remote Sens. 81 (5), 345–354.
- Inoue, Y., Sakuratani, T., Shibayama, M., Morinaga, S., 1994. Remote and real-time sensing of canopy transpiration and conductance - comparison of remote and stemflow gauge methods in soybean canopies as affected by soil-water status. Jpn. J. Crop Sci. 63 (4), 664–670.
- Jackson, R.D., Reginato, R.J., Idso, S.B., 1977. Wheat canopy temperature: a practical tool for evaluating water requirements. Water Resour. Res. 13 (3), 651–656.
- Jacob, F., et al., 2004. Comparison of land surface emissivity and radiometric temperature derived from MODIS and ASTER sensors. Remote Sens. Environ. 90 (2), 137–152.
- Jarvis, P.G., McNaughton, K., 1986. Stomatal Control of Transpiration: Scaling up from Leaf to Region, Advances in Ecological Research. Elsevier, pp. 1–49.
- Jones, H.G., 2013. Plants and Microclimate: a Quantitative Approach to Environmental Plant Physiology. Cambridge university press.
- Kalma, J.D., McVicar, T.R., McCabe, M.F., 2008. Estimating land surface evaporation: a review of methods using remotely sensed surface temperature data. Surv. Geophys. 29 (4-5), 421–469.
- Kalogirou, S.A., 2009. Solar Energy Engineering: Processes and Systems. pp. 1–762.
 Kalthoff, N., et al., 2006. The energy balance, evapo-transpiration and nocturnal dew deposition of an arid valley in the Andes. J. Arid Environ. 65 (3), 420–443.
- Klos, R.J., Wang, G.G., Bauerle, W.L., Rieck, J.R., 2009. Drought impact on forest growth and mortality in the southeast USA: an analysis using Forest Health and monitoring data. Ecol. Appl. 19 (3), 699–708.
- Kustas, W., Anderson, M., 2009. Advances in thermal infrared remote sensing for land surface modeling. Agric. For. Meteorol. 149 (12), 2071–2081.
- Kustas, W., et al., 2011. Mapping daily evapotranspiration at field to continental scales using geostationary and polar orbiting satellite imagery. Hydrol. Earth Syst. Sci. 15 (1), 223.
- Lagos, L.O., et al., 2013. Surface energy balance model of transpiration from variable canopy cover and evaporation from residue-covered or bare soil systems: model evaluation. Irrig. Sci. 31 (2), 135–150.
- Law, B., 2005. AmeriFlux US-MRf Mary's River (Fir) Site.
- Leuning, R., Foster, I.J., 1990. Estimation of transpiration by single trees comparison of a ventilated chamber, leaf energy budgets and a combination equation. Agric. For. Meteorol. 51 (1), 63–86.
- Li, F., Kustas, W.P., Prueger, J.H., Neale, C.M., Jackson, T.J., 2005. Utility of remote sensing-based two-source energy balance model under low-and high-vegetation cover conditions. J. Hydrometeorol. 6 (6), 878–891.
- Liou, Y.-A., Kar, S.K., 2014. Evapotranspiration estimation with remote sensing and various surface energy balance algorithms—a review. Energies 7 (5), 2821–2849.
- Maeda, E.E., Wiberg, D.A., Pellikka, P.K.E., 2011. Estimating reference evapotranspiration using remote sensing and empirical models in a region with limited ground data availability in Kenya. Appl. Geogr. 31 (1), 251–258.
- Maes, W.H., Steppe, K., 2012. Estimating evapotranspiration and drought stress with ground-based thermal remote sensing in agriculture: a review. J. Exp. Bot. 63 (13), 4671–4712.
- Male, D., Granger, R., 1981. Snow surface energy exchange. Water Resour. Res. 17 (3), 609-627.
- Meyers, T., 2005. AmeriFlux US-ChR Chestnut Ridge.
- Mildrexler, D.J., Zhao, M., Running, S.W., 2011a. A global comparison between station air temperatures and MODIS land surface temperatures reveals the cooling role of forests. J. Geophys. Res. Biogeosci. (G3), 116.
- Mildrexler, D.J., Zhao, M., Running, S.W., 2011b. Satellite finds highest land skin temperatures on earth. B Am. Meteorol. Soc. 92 (7), 855–860.
- Monteith, J., 1964. Evaporation and environment. Symp. Soc. Exp. Biol. 205–234.
- Mu, Q., Zhao, M., Running, S.W., 2011. Improvements to a MODIS global terrestrial evapotranspiration algorithm. Remote Sens. Environ. 115 (8), 1781–1800.
- Nagler, P.L., Glenn, E.P., Thompson, T.L., 2003. Comparison of transpiration rates among saltcedar, cottonwood and willow trees by sap flow and canopy temperature methods. Agric. For. Meteorol. 116 (1-2), 73–89.
- Nagler, P.L., et al., 2005. Predicting riparian evapotranspiration from MODIS vegetation indices and meteorological data. Remote Sens. Environ. 94 (1), 17–30.
- Noormets, A., 2005. AmeriFlux US-NC2 NC_Loblolly Plantation.
- Norman, J.M., Kustas, W.P., Humes, K.S., 1995. Source approach for estimating soil and vegetation energy fluxes in observations of directional radiometric surface temperature. Agric. For. Meteorol. 77 (3-4), 263–293.
- Norman, S.P., Koch, F.H., Hargrove, W.W., 2016. Review of broad-scale drought monitoring of forests: toward an integrated data mining approach. For. Ecol. Manag. 380, 346–358.
- Novick, K.A., et al., 2015. On the difference in the net ecosystem exchange of CO2 between deciduous and evergreen forests in the southeastern United States. Glob. Change Biol. 21 (2), 827–842.
- Oishi, C., Novick, K., Stoy, P., 2001-2008a. AmeriFlux US-Dk2 Duke Forest-hardwoods, doi:10.17190/AMF/1246047.
- Oishi, C., Novick, K., Stoy, P., 2001-2008b. AmeriFlux US-Dk3 Duke Forest loblolly pine.

- Pallas, J.E., Harris, D.G., 1964. Transpiration stomatal activity + leaf temperature of cotton plants as influenced by radiant energy relative humidity + soil moisture tension. Plant Physiol. 39, R43-&.
- Penman, H.L., 1948. Natural evaporation from open water, bare soil and grass.

 Proceedings of the Royal Society of London A: Mathematical, Physical and
 Engineering Sciences 120–145.
- Prata, A., 1996. A new long-wave formula for estimating downward clear-sky radiation at the surface. Q. J. R. Meteorol. Soc. 122, 1127–1151.
- Price, J.C., 1980. The potential of remotely sensed thermal infrared data to infer surface soil-moisture and evaporation. Water Resour. Res. 16 (4), 787–795.
- Price, J.C., 1982. Estimation of regional scale evapo-transpiration through analysis of satellite thermal-infrared data. IEEE Trans. Geosci. Remote 20 (3), 286–292.
- Priestley, C.H.B., Taylor, R.J., 1972. Assessment of surface heat-flux and evaporation using large-scale parameters. Mon. Weather Rev. 100 (2), 81-+.
- PRISM, P.C.G., 2004. In: O.S.U. PRISM Climate Group (Ed.), Monthly and Normal Air Temperature Data.
- Rahman, Mohammad A., Moser, Astrid, Rötzer, Thomas, Pauleit, Stephan, 2017. Within canopy temperature differences and cooling ability of Tilia cordata trees grown in urban conditions. Build. Environ. 114, 118–128.
- Saha, S.K., Ajai Gopalan, A.K.S., Kamat, D.S., 1986. Relations between remotely sensed canopy temperature, crop water-stress, air vapor-pressure deficit and evapotranspiration in Chickpea. Agric. For. Meteorol. 38 (1-3), 17–26.
- Sanchez, J.M., et al., 2007. Evaluation of the B-method for determining actual evapotranspiration in a boreal forest from MODIS data. Int. J. Remote Sens. 28 (6), 1231–1250
- Schwantes, A.M., et al., 2017. Measuring canopy loss and climatic thresholds from an extreme drought along a fivefold precipitation gradient across Texas. Glob. Change Biol. 23 (12), 5120–5135.
- Seguin, B., Itier, B., 1983. Using midday surface temperature to estimate daily evaporation from satellite thermal IR data. Int. J. Remote Sens. 4 (2), 371–383.
- Seyednasrollah, B., 2018. Drought eye: monitoring thermal stress in near real-time. Zenodo. https://doi.org/10.5281/zenodo.1465295.
- Seyednasrollah, B., Kumar, M., 2013. Effects of tree morphometry on net snow cover radiation on forest floor for varying vegetation densities. J. Geophys. Res. Atmos. 118 (22), 12 508-12,521.
- Seyednasrollah, B., Kumar, M., 2014. Net radiation in a snow-covered discontinuous forest gap for a range of gap sizes and topographic configurations. J. Geophys. Res. Atmos. 119 (17).
- Seyednasrollah, B., Kumar, M., Link, T.E., 2013. On the role of vegetation density on net snow cover radiation at the forest floor. J. Geophys. Res. Atmos. 118 (15), 8359–8374.
- Sobrino, J.A., et al., 2008. Land surface emissivity retrieval from different VNIR and TIR sensors. IEEE Trans. Geosci. Remote 46 (2), 316–327.
- Stone, L.R., Horton, M.L., 1974. Estimating evapotranspiration using canopy temperatures field evaluation. Agron. J. 66 (3), 450–454.
- Tang, X.G., et al., 2014. How is water-use efficiency of terrestrial ecosystems distributed and changing on Earth? Sci. Rep.-Uk 4.
- Teixeira, Ad.C., Bastiaanssen, W.G., Ahmad, M.-u.-D., Bos, M., 2009. Reviewing SEBAL input parameters for assessing evapotranspiration and water productivity for the Low-Middle Sao Francisco River basin, Brazil: part A: calibration and validation. Agric, For. Meteorol. 149 (3-4), 462–476.
- Tew, R.K., 1962. Relations Between Transpiration, Leaf Temperatures, and Some Environmental Factors.
- Timmermans, W.J., Kustas, W.P., Anderson, M.C., French, A.N., 2007. An intercomparison of the surface energy balance algorithm for land (SEBAL) and the twosource energy balance (TSEB) modeling schemes. Remote Sens. Environ. 108 (4), 369–384.
- Vose, J., Clark, J.S., Luce, C., 2016. Effects of Drought on Forests and Rangelands in the United States: A Comprehensive Science Synthesis.
- Wang, K., Dickinson, R.E., 2012. A review of global terrestrial evapotranspiration: observation, modeling, climatology, and climatic variability. Rev. Geophys. 50 (2).
- Wardlow, B., et al., 2016. Remote sensing of drought: emergence of a satellite-based monitoring toolkit for the United States. In: Thenkabail, P.S. (Ed.), Remote Sensing of Water Resources, Disasters, and Urban Studies, pp. 367–400.
- Wilber, A.C., Kratz, D.P., Gupta, S.K., 1999. Surface Emissivity Maps for Use in Satellite Retrievals of Longwave Radiation.
- Wilson, A.M., Jetz, W., 2016. Remotely sensed high-resolution global cloud dynamics for predicting ecosystem and biodiversity distributions. PLoS Biol. 14 (3).
- Yang, Y.T., Long, D., Shang, S.H., 2013. Remote estimation of terrestrial evapotranspiration without using meteorological data. Geophys. Res. Lett. 40 (12), 3026–3030.
- Zhu, J.W., Zeng, X.D., 2015. Comprehensive study on the influence of evapotranspiration and albedo on surface temperature related to changes in the leaf area index. Adv. Atmos. Sci. 32 (7), 935–942.